Ab Initio Investigations of Iron-Based Martensitic Systems

H.C. Herper, E. Hoffmann and P. Entel

Gerhard-Mercator-Universität Duisburg, Theoretische Tieftemperaturphysik, Lotharstrasse 1, 47048 Duisburg, Germany

Abstract: We apply a full-potential first-principles method to investigate the electronic-structure and elastic features of pure iron and ordered transition metal systems like Fe-Ni and Fe-Mn. The martensitic phase transformations in these compounds mainly depend on the properties of iron. Therefore the phase diagram of iron has been studied in detail in view of structural transformations and magnetic order. To this the total energy and magnetic moment have been investigated as function of the atomic volume. In agreement with experimental results, we find a ferromagnetic bcc ground-state and an antiferromagnetic fcc phase having a higher energy of 7 mRy. The resulting pressure for the bcc $\rightarrow$ hcp transition is about 11.5 GPa in agreement with experiments. Besides that, total energy calculations have been done for stoichiometric Fe-Mn and Fe-Ni compounds. The resulting alloy phase diagrams are in a good agreement with the experimental data.
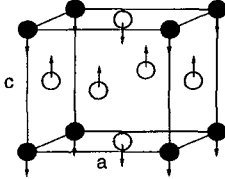
1. INTRODUCTION

In many ferrous transition metal alloys there is a strong interplay of structural and magnetic phase transitions [1]. Earlier theoretical investigations suggested that the martensitic $\gamma \rightarrow \alpha$ transformation in pure iron is driven by the onset of ferromagnetic order [2]. In this paper we try to examine in how far this iron feature is conserved in ferrous transition metal alloys. For a long time it was not possible to get a satisfying theoretical description of iron. Many methods give only a partially correct description of the sequence of energies associated with the different structural and magnetic ground states [3, 4]. In order to understand better the connection between magnetic order and structural transitions it is useful to study again iron in detail. Therefore, we made use of a full-potential band-structure theory in the density functional formalism together with the generalized gradient approximation (GGA) which provides a proper description of iron. The resulting zero temperature phase diagram compares well with experimental findings. The resulting energy differences between the different phases allow to draw some conclusions about the transition temperatures, thereby reproducing experimental results qualitatively well. Next we extended the calculations to transition metal alloys. In this paper we focus on the Fe-Mn and Fe-Ni systems with Mn and Ni having both a close-packed ground state structure but different magnetic behavior, which allows us to check the influence of iron in different magnetic environments. Because of the need of a large computational effort calculations were restricted to the fcc and bcc phases. Though manganese has a more complex structure, we still can extract chemical trends from these restricted calculations and apart from that fcc Mn is the technologically more interesting material.

2. METHOD

The structural and magnetic phase diagrams of the two martensitic systems, Fe-Ni and Fe-Mn, are obtained from full-potential energy calculations for the stoichiometric compounds Fe, Fe_3X, FeX, X [X = Ni, Mn]. We have studied the ferromagnetic (FM), nonmagnetic (NM) and antiferromagnetic

(AFM) states of these systems. In the present work the AFM state is always a layered AF1 structure, see Fig. 1. This case requires only a relatively small unit cell (4 atoms per cell) compared to other antiferromagnetic orderings.

The lattice constants, total energies and magnetic moments have been calculated within the full

Figure 1: Representation of the tetragonal unit cell (fcc: $c/a = 1.0$, bcc: $c/a = 1/\sqrt{2}$). Black and white circles mark (different) sorts of atoms. The spin order corresponds to a layered antiferromagnet.

potential linearized augmented plane-wave (FLAPW) method employing the WIEN95 code [6]. A detailed description of the method can be find in Ref. [5]. All investigations were performed using the generalized gradient approximation (GGA II) for the exchange and correlation potential established by Perdew and Wang [7]. This is unavoidable for iron rich systems as well as for iron itself, otherwise total energy calculations would produce a hexagonal ground state of iron [3].

Static ground state properties like equilibrium volume and bulk modulus B_0 were extracted from total energy calculations using fits to the Murnaghan's equation of state [8]. For more computational details see [9, 10].

3. RESULTS

3.1. Ground state properties of Mn, Fe and Ni

We start by discussing the pure transition metals. The calculated equilibrium volume V_0, saturation magnetization M_0 and bulk moduli B_0 for the bcc and fcc ground states are given in Table 1 together with the experimental values. The calculated equilibrium volumes are always smaller than the experimental ones. The maximum deviation is obtained for antiferromagnetic fcc Mn (about 7%) and fcc Fe (5.4%). This can be understood from two facts. First, we used ideal fcc and bcc lattices instead of tetragonal distorted lattices. Second, we did not take into account zero point lattice energies. For manganese there is an additional problem because the experimental equilibrium volume has been extrapolated from data corresponding to Cu-Mn, Ni-Mn and Fe-Mn alloys.

The magnetic moments of all investigated phases are in good agreement with experimental findings. The largest discrepancy occurs for AFM γ-Fe, however the value cited in Table 1 is only a lower limit for the magnetic moment of AFM fcc Fe [15]. Summarizing we can say that the ground state properties of Mn, Fe and Ni are well reproduced.

In the following we will discuss the iron phase diagram in detail (see Fig.1) baring in mind that the martensitic phase transformations of Fe-Ni and Fe-Mn occur in the iron rich region. In agreement with experiment we found a ferromagnetic bcc ground state. The lowest lying fcc phase has antiferromagnetic order and is about 7.1 mRy higher in energy than the FM bcc state. This energy difference can be related to the experimental $\alpha \rightarrow \gamma$ transition temperature T_0. Furthermore a nonmagnetic hcp state exists 6 mRy above the bcc ground state having an equilibrium volume of $V_0 = 69.94$ a.u. The calculated transition pressure amounts to 11.5 GPa which is comparable to the experimental value of 13.6 GPa. The ferromagnetic fcc phase has two local minima, a low-moment low-spin state (LS) and a high-moment high-spin (HS) state. Especially the HS state is important for the discussion of magnetovolume instabilities in iron. From this the Anti-Invar effect can be understood as a transition from AFM γ-Fe to FM HS γ-Fe caused by thermal excitations. This is connected to a volume expansion of about 12.5% compared to the experimentally observed value of

Table1: Calculated atomic volume (V_0), bulk modulus (B_0) and magnetic moment (M_0) for the ground states of the fcc and bcc structure. Additionally the hcp data of iron are presented. Experimental data are given in brackets. All theoretical results are calculated with the FLAPW method using GGA.

System	Structure		$V_0/\mathrm{atom(a.u.}^3)$	$B_0(Mbar)$	$M(\mu_B)$
Mn	bcc	FM	73.98	2.53	1.00 $(1.00)^a$
	fcc	AFM	76.79 $(82.70)^b$	1.51	1.90 $(2.40)^a$
Fe	bcc	FM	76.95 $(78.94)^c$	1.86 $(1.68)^d$	2.17 $(2.22)^d$
	fcc	AFM	72.16 $(76.24)^c$	1.93	1.30 $(0.75)^e$
	hcp	NM	69.64 $(70.51)^f$	2.91 $(2.05)^f$	0.00
Ni	bcc	FM	74.23	1.88	0.52
	fcc	FM	73.43 $(73.65)^c$	2.00 $(1.86)^c$	0.60 $(0.61)^c$

^{a} Reference [12]

^{b} Reference [16](Lattice constant extrapolated to $T = 0$ K)

^{c} Reference [13] (Lattice constant extrapolated to $T = 0$ K)

^{d} Reference [14] (Bulk modulus at T_R, magnetic moment at $T = 0$ K)

^{e} Reference [15] (Magnetic moment below T_N.)
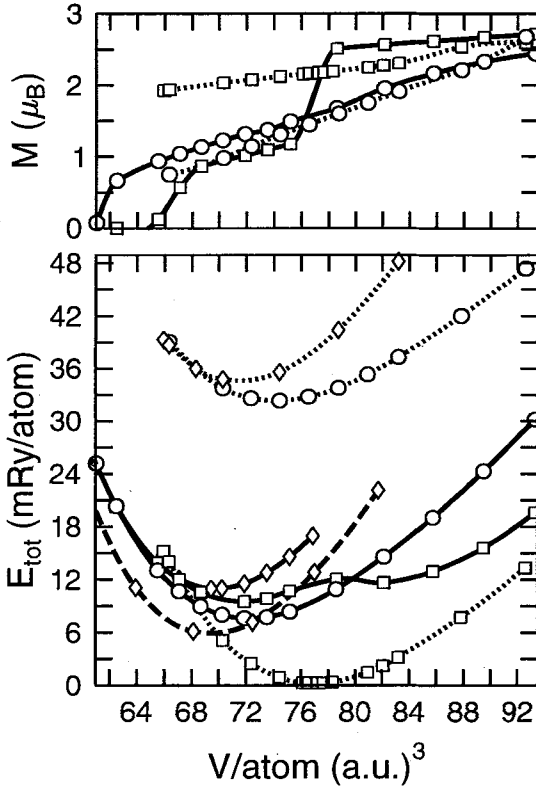
^{f} W. Pepperhoff, unpublished

14% [13]. From the results given in Fig. 2 we can conclude that the full potential LAPW method is correct for iron. It gives a good description of the structural and magnetic phases with the main results being in a good agreement with the experimental findings. Similar investigations have been done for nickel and manganese. Some of the most important results have already been mentioned (see Table 1). Nickel can be dealt with by using any band-structure theory. The same is correct for the structural states of manganese, but the description of the magnetic phases is improved by the full-potential method compared to methods without a self-interaction correction.

In the following part we will focus on the concentration dependent phase diagrams of the Fe-Mn and Fe-Ni systems. From the total energies and magnetic moments for several stoichiometric ordered systems we extracted the concentration dependent structural phase diagram of these systems.

3.2. Fe-Ni

The theoretical and experimental phase diagram of the Fe-Ni alloy is given in Fig. 3. The most important result is connected with the energy difference $\Delta E_{\mathrm{fcc-bcc}}$ between the fcc and bcc ground state, which can be related to the martensitic transition temperature. For $x \leq 70$ at% Fe the close-packed phase is always stable. Systems with larger iron concentrations prefer a bcc ground state. This is in excellent agreement with the experimental results, see left panel in Fig. 3. The absolute values of the transition temperatures can not be determined from our theoretical work. The behavior of the magnetic moments is comparable with experiment. M_γ increases from 0.5 μ_B for Ni to 2 μ_B for 70 at% Fe. For larger iron concentrations the magnetic moment of the γ phase shrinks. That is connected with the onset of the martensitic phase transformation. In contrast to experiments we can simulate each phase over the whole concentration range and calculate M_γ for fcc iron. But as can be seen in Fig. 2, this fcc phase is then higher in energy than bcc iron. On the Ni-rich side the magnetic moment compares qualitatively well with experiment. For iron it is known that bcc iron is stabilized by the ferromagnetic order (see section 3.1). The nonmagnetic and antiferromagnetic solutions have much higher energy. Without magnetism fcc would be always stable. We can conclude that there would be no martensitic $\alpha \rightarrow \gamma$ transformation without the magnetic order of iron.

Furthermore we have calculated the energy differences between ferromagnetic, antiferromagnetic and nonmagnetic fcc phases of Fe-Ni. $\Delta E^{\mathrm{fcc}}_{\mathrm{FM-NM}}$ is a rough measure for the Curie temperature T_C^γ.
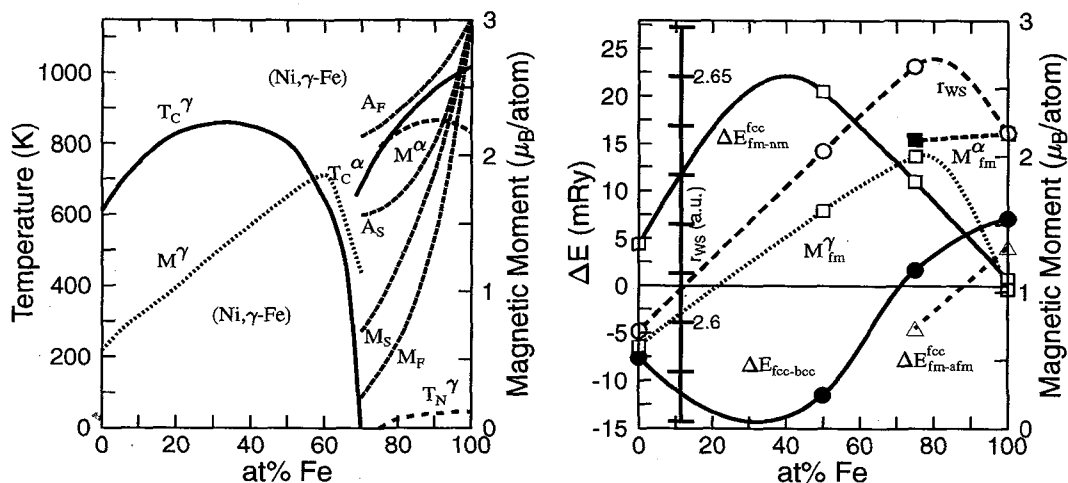
Figure 2: Total energies E_{tot} (lower panel) and magnetic moments M (upper panel) of iron obtained from FLAPW calculations within the GGAII. Results are shown for the fcc and bcc crystal structure and different magnetic ordering. Additionally the nonmagnetic hcp curve is presented (dashed line with diamonds). The solid curves corresponds to the fcc phase, and the dotted to the bcc phase. The diamonds indicate the nonmagnetic, the squares ferromagnetic and circles the antiferromagnetic order. For the ferromagnetic fcc phase exists a high-spin solution at $V_0^{HS} = 81.15$ a.u. and a low-spin state at $V_0^{LS} = 71.69$ a.u. The sequence of the magnetic states of the fcc phase is important for the discussion of the Anti-Invar effect. This magneto-volume effect can be explained by thermal excitations from the AFM ground state to the high-volume HS FM state. The volume expansion is about 12.5% being close to the experimentally observed one.

The shape of the theoretical and experimental curves are identical as long as the fcc phase is the ground state. For larger iron concentrations it is not possible to measure T_C^γ. The Neél temperature, which can be described by ΔE_{FM-AFM}^{fcc}, shows also a qualitatively correct behavior. But in this case the calculated stability range is smaller. Only for iron concentrations larger than 87 at% Fe the AFM state is stable, whereas in nature AFM ordering is possible at lower iron concentration. The last point to discuss is the concentration dependence of the Wigner-Seitz Radius r_{WS}. The maximum of the r_{WS} is found in the martensitic region about 80 at% Fe, whereas the maximum of the experimental curve occurs at 61 at% Fe (Invar region). The shift to larger r_{WS} may be caused by the stoichiometric order used in our calculations.
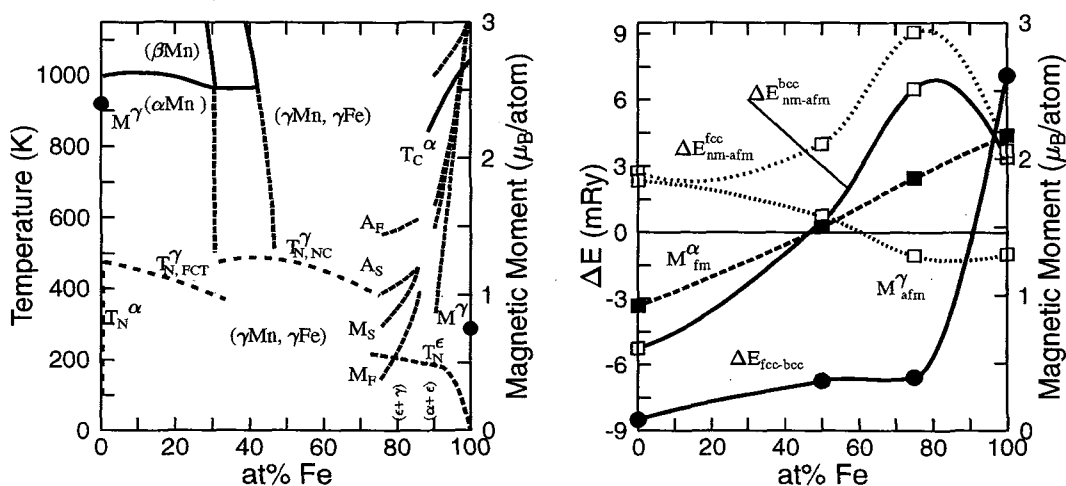
3.3. Fe-Mn

For the Fe-Mn system similar calculations have been done. The results are given in Fig. 4. In contrast to the Fe-Ni compound, antiferromagnetism in Fe-Mn is more important, because both Fe and Mn, have an AFM fcc ground state. Again M_γ follows the right chemical trend, but the absolute values obtained are slightly too large.

We found that for systems containing less than 80 at% Fe the fcc phase is stable, larger iron concentrations leads to a bcc-like ground state. In nature only systems with more than 90 at% Fe have a bcc ground state. For systems with Fe concentrations between 80 and 90 at% a hcp→fcc transformation plays an important role in the Fe-Mn system.

Figure 3: Experimental (left) and theoretical (right) phase diagram of Fe-Ni. The labels γ, α refer to the fcc, bcc structures. Temperatures in the left figure are Curie (T_C) and Néel (T_N) temperatures. Austenite/martensite start and final temperatures are labeled by A_F, A_S, M_S, M_F. M^γ (M^α) denotes the saturation magnetization of the fcc (bcc) phase. The theoretical energy differences can be compared with the temperatures in the left panel. ΔE_{NM-FM}^{fcc} is correlated to T_C^γ and ΔE_{FM-AFM}^{fcc} simulates T_N^γ. $\Delta E_{fcc-bcc}$ determines the stability range of an fcc ground state. The inset scale in the right panel belongs to the Wigner-Seitz radius r_{WS} (dashed line with open circles). For details see text.

Figure 4: Experimental (left) and theoretical (right) phase diagram of Fe-Mn. The labels γ, α refer to the fcc, bcc structures. The temperatures on the left figure are Curie (T_C) and Néel (T_N) temperatures. Austenite/martensite start and final temperatures are labeled by A_F, A_S, M_S, M_F. M^γ denotes the saturation magnetization of fcc Mn and fcc Fe. The theoretical energy differences can be compared to the temperatures in the left panel. ΔE_{NM-AFM}^{fcc} is correlated to T_N^γ. $\Delta E_{fcc-bcc}$ determines the stability range of an fcc ground state. For more information see text.

This can not be seen in the theoretical phase diagram, where hcp·or mixed phases have not been considered. Additionally we have examined total energy differences of the magnetic phases. We found a weak concentration dependence of the Neél temperature being correlated to ΔE_{NM-AFM}^{fcc}. This agrees with the experimental observations (see Fig. 4).

4. CONCLUSIONS

In this paper we have presented theoretical phase diagrams for two transition metal alloys. Though only four stoichiometric ordered systems have been calculated, we can draw some interesting conclusions from the results mentioned above. Characteristic features of iron still exist in Fe-Ni alloys in the martensitic region. In systems containing more than 70 at% iron the structural as well as the magnetic properties are dominated by FM bcc iron. However, the Fe-Mn system behaves differently. First, this system is nearly AFM for all concentrations, because antiferromagnetism is favored by Mn. On the other hand antiferromagnetism prefers close packed structures. From our calculations we may conclude that the bcc phase of Fe-Mn is already destabilized for Fe concentrations less than 90 at%, which does qualitatively agree with experiments. The reason that bcc Fe-Mn exist only in a small concentration region, is the AFM character of Mn, because bcc is only stabilized through FM (see section 3.2.).

At least one should keep in mind that only cubic phases are discussed though these alloys show also $\alpha \rightarrow \epsilon$ transitions. This will be discussed in a forthcoming paper.

References

[1] Wassermann E.F., Ferromagnetic Materials (North-Holland, Amsterdam, 1990) , pp. 240.
[2] Moruzzi V.L., Marcus P.M., Schwarz K., and Mohn P., *Phys. Rev. B* **34** (1986) 1784-1791.
[3] Asada T. and Terakura K., *Phys. Rev. B* **46** (1992) 13599-13602.
[4] Wang C.S., Klein B.M., and Krakauer H., *Phys. Rev. Lett.* **54** (1985) 1852-1855.
[5] Singh D.J., Planewaves, Pseudopotentials and the LAPW method (Kluwer Acad., Boston, 1994).
[6] Blaha P., Schwarz K., Dufek P., and Augustyn R., WIEN95, TU of Vienna 1995. (Improved and updated Unix version of the original copyrighted WIEN-code, published by Blaha P., Schwarz K., Sorantin P., and Trickey S.B., in *Comput. Phys. Commun.* **59** (1990) 399).
[7] Perdew J.P., and Wang Y., *Phys Rev. B* **45** (1992) 13244-13249.
[8] Murnaghan F.D., *Proc. Nat. Acad. Sci. USA* **30** (1944) 244-247.
[9] Herper H.C., Hoffmann E., and Entel P., "Ab initio investigations of phonon anomalies and martensitic transformations", IAC1, Athens 16-21 June 1996, Plenum, in press.
[10] Herper H.C., Hoffmann E. and Entel P., in preparation
[11] Donohue J., The structures of the elements (Robert Krieger Publ., Florida, 1982) pp. 198-200.
[12] Tebble R.S., Craik D.J., Magnetic Materials (Wiley & Sons, London,1969), p. 62.
[13] Acet M., Zähres H., and Wassermann E.F., *Phys. Rev. B* **49** (1994) 6012.
[14] Kittel C., Introduction to Solid State Physics (Wiley & Sons, New York, 1971, 4th ed.) pp. 143+536.
[15] Abrahams S.C., Guttman L., and Kasper J.S.,*Phys. Rev* **127** (1962) 2052-2055.
[16] Acet M., Zähres H., Stamm W., Wassermann E.F., and Pepperhoff W., *Physica B* **161** (1989) 67-71.